Ruthenocene-Containing β-Diketones: Synthesis, pK_a' Values, Keto–Enol Isomerization Kinetics, and Electrochemical Aspects

K. Christian Kemp, Eleanor Fourie, Jeanet Conradie, and Jannie C. Swarts*

Department of Chemistry, University of the Free State, P.O. Box 339, Bloemfontein 9300, Republic of South Africa

Received June 20, 2007

Claisen condensation of acetyl ruthenocene with the appropriate methyl ester, RCOOMe, under the influence of the hindered base lithium diisopropylamide gave the β-diketones ($RcCOCH_2COR$) 1-ruthenocenyl-4,4,4-trifluorobutane-1,3-dione (ruthenocenoyltrifluoroacetone, **1**, R = CF_3; pK_a' = 7.36 ± 0.03), 1-ruthenocenylbutane-1,3-dione (ruthenocenoylacetone, **2**, R = CH_3; pK_a' = 10.22 ± 0.01), 1-phenyl-3-ruthenocenylpropane-1,3-dione (benzoylruthenocenoylmethane, **3**, R = C_6H_5; pK_a' = 11.31 ± 0.03), 1-ferrocenyl-3-ruthenocenylpropane-1,3-dione (ferrocenoylruthenocenoylmethane, **4**, R = Fc = $(C_5H_5)Fe(C_5H_4)$ = ferrocenyl; pK_a' = ca. 12.8), and 1,3-diruthenocenylpropane-1,3-dione (diruthenocenoylmethane, **5**, R = Rc = $(C_5H_5)Ru(C_5H_4)$ = ruthenocenyl; pK_a' = ca. 12.7). The group electronegativity of the ruthenocenyl group, χ_{Rc} = 1.89 on the Gordy scale, was obtained from the linear relationship between IR carbonyl stretching frequencies of a series of methyl esters, RCOOMe, and χ_R. A ^{1}H NMR kinetic study of the enol−keto interconversion resulted in accurate equilibrium constants, K_c, for this equilibrium, as well as forward and reverse rate constants of the isomerization process. Cyclic voltammetry in $CH_3CN/N(^nBu)_4PF_6$ utilizing a glassy-carbon electrode showed the ruthenocene center exhibited, in contrast to the ferrocene center, irreversible electrochemistry. The multiple peak anodic (oxidation) potentials observed are a consequence of slow isomerization kinetics and made peak assignments for the keto and enol isomers possible. The kinetics of enol to keto isomerization for **4** was also studied by cyclic and Osteryoung square wave voltammetry; obtained rate constants were mutually consistent with those obtained by the ^{1}H NMR technique. Kinetic rate constants, K_c, and pK_a' and $E_{p,a}$ were related to χ_R values of the R groups in $RcCOCH_2COR$.

Introduction

β-Diketones and their metal complexes have been the subject of many kinetic,[1] catalytic,[2] and medical studies.[3,4] Ruthenocene-containing compounds have been investigated as imaging agents,[5] for photoelectrochemical uses,[6] and as surfactants,[7] as well as for other beneficial uses.[8] Ruthenocene organic chemistry parallels that of ferrocene. However, the cyclopentadienyl (Cp = $C_5H_5^-$) ligands of ruthenocene are much more resistant toward aromatic substitution reactions than are those of ferrocene. Consequently, the organic chemistry of ruthenocene has not been reported on as comprehensively. Due to the fact that ruthenium compounds prevent, or at least minimize, cytotoxicity induced by other chemotherapeutic drugs,[9,10] we were interested in synthesizing and characterizing some hitherto unknown ruthenocene-containing β-diketones. These complexes may show appreciable antineoplastic activity.

Methods used in β-diketone synthesis are wide and varied,[11,12] but Cullen's[13] use of lithium diisopropylamide as a base during the Claisen condensation of ketones with esters has been used with considerable success for ferrocene-containing β-diketones.[14] β-Diketone yields were substantially better than those obtained when condensations were performed under the influence of $NaNH_2$, KNH_2, or NaOMe.[15]

Regarding the equilibrium between β-diketone keto and enol isomers, two driving forces, the electronic driving force and the resonance driving force, were described[14,16,17] that will determine the dominant enol isomer in solution. On the basis

* To whom correspondence should be addressed. E-mail: swartsjc.sci@ufs.ac.za.

(1) Moon, S.; Kwan, Y. *Magn. Reson. Chem.* **2001**, *39*, 89.
(2) Cullen, W. R.; Rettig, S. J.; Wickenheimer, E. B. *J. Mol. Catal.* **1991**, *66*, 251.
(3) Bennet, I.; Broom, N. J. P.; Cassels, R.; Elder, J. S.; Masson, N. D.; O'Hanlon, P. J. *Bioorg. Med. Chem. Lett.* **1999**, *9*, 1847.
(4) (a) Mehrotora, R. C.; Bohra, R.; Gaur, D. P. In *Metal β-Diketonates and Allied Derivatives*; Academic Press: London, 1978; p 268. (b) Stray, J. In *The Solvent Extraction of Metal Chelates*; Macmillan: New York, 1964; pp 51–55. (c) Marcus, Y.; Keates, A. S. In *Ion Exchange and Solvent Extraction of Metal Complexes*; Wiley-Interscience: New York, 1969; pp. 499–521.
(5) (a) Herken, R.; Wenzel, M. *Eur. J. Nucl. Med.* **1985**, *10*, 56. (b) Shani, J.; Livshitz, T.; Wenzel, M. *Int. J. Nucl. Med. Bio.* **1985**, *12*, 13.
(6) Blake, A. J.; Mayers, F. R.; Osborne, A. G.; Rosseinsky, D. R. *J. Chem. Soc., Dalton Trans.* **1982**, 2379.
(7) Jacob, C.; Safronov, A. Y.; Wilson, S.; Hill, H. A. O.; Booth, T. F. *J. Electroanal. Chem.* **1997**, *427*, 161.
(8) (a) Beagley, P.; Blackie, M. A. L.; Chibale, K.; Clarkson, C.; Moss, J. R.; Smith, P. J. *Dalton Trans.* **2002**, 4426. (b) Miura, H.; Taguchi, H.; Sugiyama, K.; Matsuda, T.; Gonzalez, R. D. *J. Catal.* **1990**, *124*, 194.
(9) Tsuruo, T.; Iida, H.; Tsukagoshi, S.; Sakuari, Y. *Biochem. Pharm.* **1981**, *30*, 213.
(10) Conter, V.; Beck, W. T. *Biochem. Pharm.* **1983**, *32*, 723.
(11) March, J. In *Advanced Organic Chemistry*, 4th ed.; Wiley:New York, 1992; p 1072.
(12) Umetani, S.; Kawase, Y. H.; Le, Q. T.; Matusi, M. *Dalton Trans.* **2000**, 2787.
(13) Cullen, W. R.; Wickenheiser, E. B. *J. Organomet. Chem.* **1989**, *370*, 141.
(14) Du Plessis, W. C.; Vosloo, T. G.; Swarts, J. C. *J. Chem. Soc., Dalton Trans.* **1998**, 2507.
(15) (a) Cain, C. E.; Mashburn, T. A., Jr.; Hauser, C. R *J. Org. Chem.* **1961**, *26*, 1030. (b) Weinmayr, V. *Naturwissenchaften* **1958**, *45*, 311.
(16) Du Plessis, W. C.; Erasmus, J. J. C.; Lamprecht, G. J.; Conradie, J.; Cameron, T. S.; Aquino, M. A. S. Swarts, J. C. *Can. J. Chem.* **1999**, *77*, 378.

10.1021/om700609z CCC: $40.75
Publication on Web 01/17/2008

Scheme 1. Synthesis of β-Diketones 1–5[a]

[a] Only the expected dominant enol isomer is shown. Fc = ferrocenyl, Rc = ruthenocenyl, LiDPA = lithium diisopropylamide.

of the electronic driving force, if $\chi_{R^2} > \chi_{R^1}$ (χ_R = group electronegativity of R groups), the enol isomer $R^1C(OH)$=$CHCOR^2$ in the equilibrium below should dominate because the C atom adjacent to R^1 will be more negative in character than the C atom next to R^2. On the basis of the resonance driving force, if R^1 is an aromatic substituent, such as ferrocenyl, phenyl, or ruthenocenyl, and R^2 is not, then R^1COCH=$C(OH)R^2$ should be the dominant enol isomer even though R^1 may be more electron-donating than R^2. Resonance stabilization may be visualized in terms of the canonical structural fragments $\mathbf{R^1(C{=}O)-} \leftrightarrow \mathbf{(R^{1,+})}$=$\mathbf{(CO^-)-}$ that may be written for the keto portion of the enol isomer $\mathbf{R^1CO}CH$=$C(OH)R^2$.

The rate of conversion between enol isomers is normally very fast, with half-lives in the microsecond range[18] not uncommon. In contrast, conversion between enol and keto isomers may take place over days.[17]

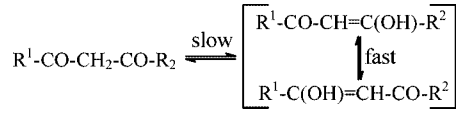

Traditionally the view has been that electrochemical oxidation of ruthenocene proceeds by a 2e irreversible process[19,20] in acetonitrile/tetrabutylammonium perchlorate. It was later shown that a 1e reversible electrochemical process occurs when the electrochemistry is performed utilizing a weakly nucleophilic electrolyte such as tetrabutylammonium tetrakis[3,5-bis(trifluoromethyl)phenyl]borate in the poorly coordinating solvent dichloromethane.[20] Under these conditions, a formal reduction potential of 1.03 V versus AgCl/Ag (1.0 M KCl) (0.57 V versus Fc/Fc^+) was obtained.

Here we report the syntheses and characterization of some new ruthenocene-containing β-diketones. Keto–enol equilibrium constants, the kinetics of isomerization, and the electrochemical properties of each ligand are also presented.

Results and Discussion

Syntheses. The β-diketones $RcCOCH_2COR$ with R = CF_3 (**1**), CH_3 (**2**), C_6H_5 (**3**), Fc (ferrocenyl, $FeCp(C_5H_4)$; **4**), Rc (ruthenocenyl, $RuCp(C_5H_4)$; **5**) were synthesized according to Scheme 1. Compound **1** was obtained in the highest yield. Due to increased acid and base instability in moving from **1** to **5**, yields systematically became lower for the other complexes. In the solid state, all β-diketones were found to convert quantitatively to the enol isomer upon aging for 3 months or longer. However, once they were dissolved in $CDCl_3$, keto isomers were found to form at slow but different rates. Once the dynamic equilibrium position has been reached in 1–4 days, no further ^1H NMR spectral changes could be observed. In analogy to analogous ferrocene β-diketones,[16,21] we assume that the solid-state enol isomer in the present compound series will be RcCOCH=C(OH)R as a result of the resonance driving force involving molecular fragments such as Rc^+=$(CO^-)-$. In solution, the same isomer is expected to dominate.

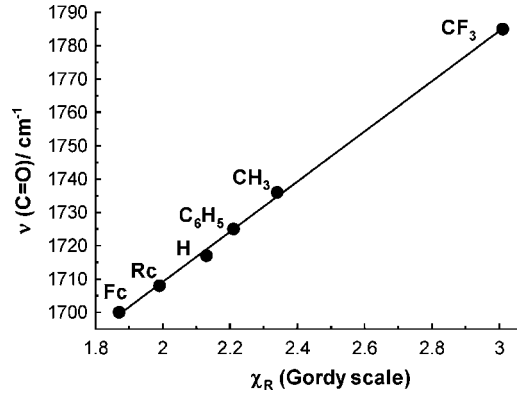

Figure 1. Plot of IR carbonyl stretching frequencies versus group electronegativities, χ_R, on the Gordy scale for a range of methyl esters, RCOOMe. The R groups are indicated on the graph.

Group Electronegativities, χ_R. We have already reported χ_R values on the Gordy scale[22] for each R group except the ruthenocenyl group of the present study.[14,16] Gordy scale χ_R values are empirical numbers that express the combined tendency of not only one atom but also a group of atoms, such as CF_3 in the present β-diketones, to attract electrons (including those in a covalent bond) as a function of the number of valence electrons, n, and the covalent radius, r (in Å), of groups as discussed elsewhere.[22] They are empirically adjusted to be aligned with Pauling atomic electronegativities. To determine the apparent χ_{Rc} value, the IR carbonyl stretching frequency of RcCOOMe was inserted in the linear plot of carbonyl stretching frequencies of a series of other methyl esters, RCOOMe, and χ_R (Figure 1). χ_{Rc} was then calculated from the manipulated equation of the graph, $\chi_R = 0.0133[\nu(C{=}O)] - 20.78$ as $\chi_{Rc} = 1.92$ on the Gordy scale. Electrochemical measurements (see below) gave $\chi_{Rc} = 1.86$. These two values are mutually consistent and average to 1.89. Literature values of 2.27 and 2.08 were reported for the ruthenocenyl and ferrocenyl groups, respectively, but it is uncertain what scale and/or conditions were used.[23]

(17) Du Plessis, W. C.; Davis, W. L.; Cronje, S. J.; Swarts, J. C. *Inorg. Chim. Acta* **2001**, *314*, 97.
(18) Iglisias, E. *J. Org. Chem.* **2003**, *68*, 2680.
(19) Kuwana, T.; Bublitz, D. E.; Hoh, G. *J. Am. Chem. Soc.* **1960**, *82*, 5811.
(20) Hill, M. G.; Lamanna, W. M.; Mann, K. R. *Inorg. Chem.* **1991**, *30*, 4687.
(21) Bell, W.; Crayston, J. A.; Glidewell, C.; Mazid, M. A.; Hursthouse, M. B. *J. Organomet. Chem.* **1992**, *434*, 115.
(22) (a) Wells, P. R. In *Progress in Physical Organic Chemistry*; Wiley: New York, 1968; Vol. 6, pp 111–145. (b) Kagarise, R. E. *J. Am. Chem. Soc.* **1955**, *77*, 1377.
(23) Bennett, M. A.; Bruce, M. I. In *Comprehensive Organometallic Chemistry*; Wilkinson, G., Stone, F. G. A., Abel, E., Eds.; Pergamon Press: Oxford, U.K., 1982; Vol. 4, pp 759–773.

Table 1. Group Electronegativities, Equilibrium Constants, Gibbs Energies (kJ mol^{-1}), Kinetic Rate Constants (s^{-1}), and Half-Lives (s) for Equilibrium (2) at 293 K

compd (solvent, technique used)	χ_R	K_c[a]	$\Delta G°$	% enol	$t_{1/2}$[b]	$10^5 k_{obsd}$[c]	$10^5 k_1$	$10^6 k_{-1}$
1, R = CF_3 ($CDCl_3$, ^{1}H NMR)	3.01	12.3	−6.1	92.5	31900	2.17(5)	2.01	1.6
2, R = CH_3 ($CDCl_3$, ^{1}H NMR)	2.34	2.2	−1.9	68.5	700	98(2)	68.3	297
3, R = Ph ($CDCl_3$, ^{1}H NMR, χ_{Ph} = 2.43[d])	2.21[d]	5.7	−4.2	85.0	11000	6.3(5)	5.36	9.4
4, R = Fc ($CDCl_3$, ^{1}H NMR)	1.87	0.9	0.3	47.0	650	107(3)	50.7	563
4, R = Fc (CD_2Cl_2, ^{1}H NMR)	1.87	1.00	0.0	50.1	470	147(9)	73.6	734
4, R = Fc (CD_2Cl_2 + electrolyte,[e] ^{1}H NMR)	1.87	1.01	−0.02	50.2	540	128(8)	64.3	637
4, R = Fc (CD_3CN, ^{1}H NMR)	1.87	0.74	−0.7	42.5	7600	9.1(5)	3.9	52
4, R = Fc (CH_3CN + electrolyte,[e] CV-Rc_{waves})	1.87	1.17	−0.4	54.0	6930	10.0(6)	5.4	46
4, R = Fc (CH_2Cl_2 + electrolyte,[e] CV-Rc_{waves})	1.87	1.38	−0.8	58	220	310(5)	180	1300
4, R = Fc (CH_2Cl_2 + electrolyte,[e] CV-Fc_{waves})	1.87	1.50	−1.0	60.0	240	290(3)	174	1160
4, R = Fc (CH_2Cl_2 + electrolyte,[e] SW-Fc_{waves})	1.87	1.09	−0.2	52.2	220	310(2)	162	1480
5, R = Rc ($CDCl_3$, ^{1}H NMR)	1.89	0.70	0.9	41.2	220	320(10)	132	1880

[a] To determine K_c, the following NMR signals (ppm) were averaged for use in eq 5: for **1**, those of COCHCO at 6.03 and $COCH_2CO$ at 3.00, and those of C_5H_5 at 4.63 and 4.70; for **2**, those of COCHCO at 5.64 and $COCH_2CO$ at 3.73, those of C_5H_5 at 4.59 and 4.61, and those of CH_3 at 2.31 and 2.05; for **3**, those of COCHCO at 6.28 and $COCH_2CO$ at 4.25, and those of C_5H_5 at 4.59 and 4.48; for **4**, those of COCHCO at 5.91 and $COCH_2CO$ at 2.28, and those of C_5H_2 (from the substituted Cp ring) at 5.19 and 5.24; for **5**, those of COCHCO at 5.83 and $COCH_2CO$ at 3.88, and those of C_5H_2 (from the substituted Cp ring) at 5.17 and 5.23. [b] Calculated from $t_{1/2} = \ln 2/k_{obs}$. [c] Values in parentheses indicate errors in the last digit(s). Not all errors are known, because the error in K_c is unknown. [d] The value of $\chi_{Ph} = 2.21$ does not appear to fit the kinetic trends of this study well. It looks as if χ_{Ph} should be larger than $\chi_{CH3} = 2.34$. A literature value of $\chi_{Ph} = 2.43$ was reported utilizing IR data for $O{=}PR_3$,[14,22] but as all other χ_R values originate from RCOOMe esters, we are content with the value of 2.21. [e] Abbreviations and conditions: electrolyte = $[N(^nBu_4)][B(C_6F_5)_4]$ = 5[**4**] = 8.75 × 10^{-2} M for ^{1}H NMR, 0.1 M in CH_2Cl_2 for CV or SW techniques, or "electrolyte" = $[N(^nBu_4)][PF_6]$ = 0.1 M in CH_3CN for the CV technique,; CV = cyclic voltammetric technique, SW = Osteryoung square wave technique.

Equilibrium Constants, K_c. To determine K_c, the equilibrium percentage of keto isomers present in $CDCl_3$ solutions for each β-diketone was first determined by comparing the relative intensities of appropriate enol/keto ^{1}H NMR signal pairs. Once the percentage of the keto isomer was known, the equilibrium constant

$$K_c = \frac{[\text{enol isomer(s)}]}{[\text{keto isomer}]} = \frac{k_1}{k_{-1}} \quad (1)$$

for the equilibrium (2) in $CDCl_3$ solutions could be evaluated.

$$\text{RcCOCH}_2\text{COR} \underset{k_{-1}}{\overset{k_1}{\rightleftharpoons}} \text{RcCOCH=C(OH)R} \quad (2)$$

The results are summarized in Table 1. A general trend that larger χ_R values lead to a slight increase in K_c values was noted, but no clear linear relationship exists between these two quantities.

Gibbs energies for the isomerization reaction (2) was obtained by application of eq 3.[17]

$$\Delta G^\circ = -RT \ln K_c \quad (3)$$

It is obvious from Table 1 that more negative Gibbs energies lead to a larger enol content at equilibrium. This is thermodynamically sound because larger negative Gibbs energies imply the thermodynamic driving force to the right of equilibrium (2) increases.

Isomerization Kinetics Utilizing ^{1}H NMR Spectroscopy. Since it was found that, at equilibrium, **2**−**5** have measurable quantities (>15%) of the keto isomer in $CDCl_3$ solutions, a first-order treatment of time-based ^{1}H NMR data showing the formation of keto isomers from aged samples was possible. ^{1}H NMR spectra of **3** in the enol form and **3** at equilibrium with ca. 15% in the keto form are shown in Figure 2. Kinetic data were obtained by monitoring the growth of the keto peaks, labeled as "k". Compound **1**, however, contained at equilibrium only 7.5% keto isomer (Table 1). This was too little to follow time-based enol to keto conversions with accuracy by ^{1}H NMR. Consequently, a keto-enriched sample was studied by following the forward reaction (i.e., keto isomer disappearance) in equilibrium (2). This is shown in Figure 3. The insert confirms the first-order behavior of this isomerization process, and the slope of this graph corresponds to $k_{obsd} = k_1 + k_{-1}$.

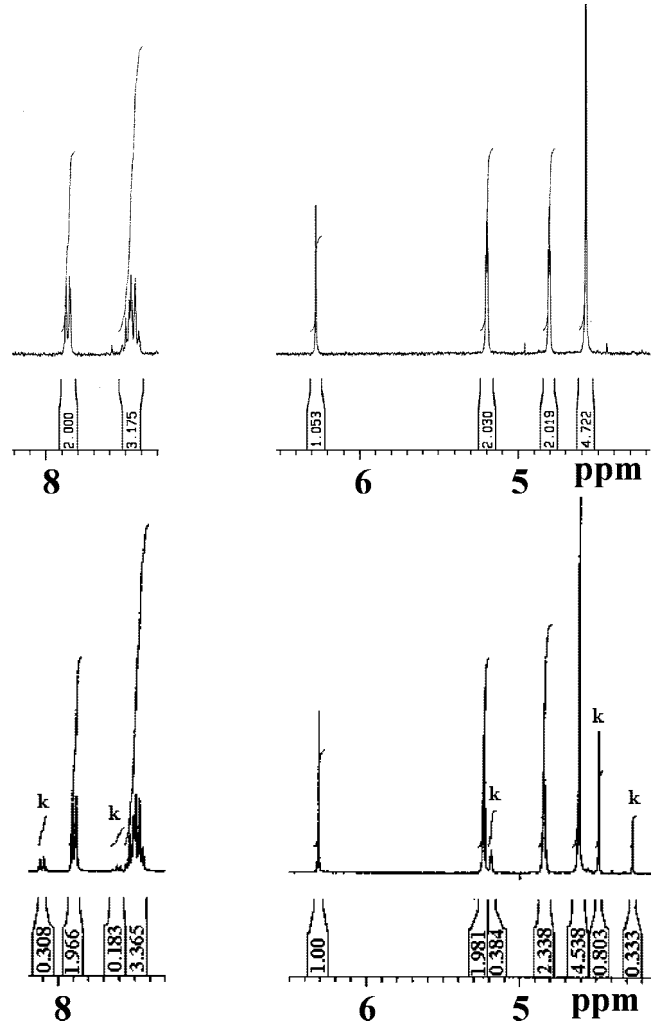

Figure 2. ^{1}H NMR spectra of **3** in the enol form (above) and at equilibrium (below) at 293 K in $CDCl_3$. The equilibrium keto content is 14–15%, and keto signals are designated by "k". Peak assignments can be found in the Experimental Section.

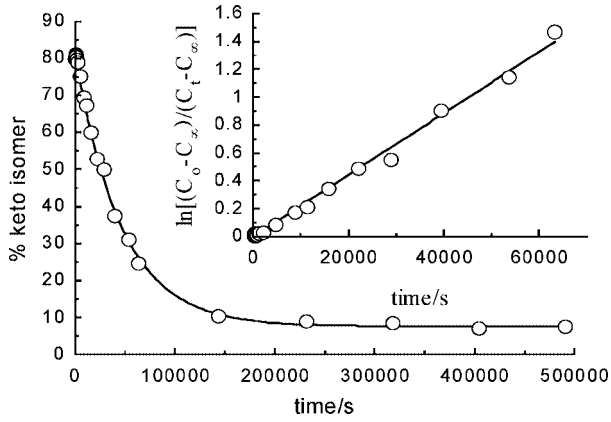

Figure 3. ^{1}H NMR determined time trace showing the conversion from keto to enol isomer for **1** at 293 K in $CDCl_3$. Insert: a kinetic first-order treatment of data for this process utilizing eq 8. *C* donates the concentration, expressed as percent keto isomer.

Since the equilibrium constant for eq 2 is known, it was possible to separate rate constants for the forward k_1 step and reverse k_{-1} step. Rate constants are summarized in Table 1. The isomerization kinetics activity series in $CDCl_3$ of the present β-diketones is as follows (compare half-lives, Table 1): (fastest) **5** (R = Rc) > **4** (R = Fc) > **2** (R = CH_3) >> **3** (R = Ph) > **1** (R = CF_3) (slowest).

Group electronegativities played an important role in isomerization kinetics. Both k_1 and k_{-1} increase with decreasing χ_R (Table 1). The reverse reaction rate in equilibrium (2), however, increases 5 times (for **2**) to 18 times (for **5**) faster than the forward reaction rate, which also explains from a kinetic point of view why $K_c = k_1/k_{-1}$ decreases with decreasing χ_R.

Although a detailed ^{1}H NMR solvent study for all compounds was not performed, the effect of $CDCl_3$ (dielectric constant 4.8), CD_2Cl_2 (dielectric constant 8.9), and CD_3CN (dielectric constant 37.5) on the equilibrium position and isomerization kinetics of **4** were investigated. The effect was very small. The general trend that the CD_3CN result suggests is that an increase in dielectric constant slightly favors the keto form of $RcCOCH_2COFc$ (i.e., leads to smaller K_c values, Table 1). Addition of a noncoordinating electrolyte such as tetrabutylammonium tetrakis(pentafluorophenyl)borate had virtually no influence on the equilibrium position of $RcCOCH_2COFc$. This result is important for the electrochemistry described below, since it shows that the presence of this electrolyte will not interfere with the isomerization process when it is studied electrochemically. In terms of how fast the equilibrium sets in, reaction half-life values ($t_{1/2}$ = ln $2/k_{obsd}$) in Table 1 indicate the overall isomerization process is the slowest in CD_3CN ($t_{1/2}$ = 7600 s), but the difference in $t_{1/2}$ for $CDCl_3$ (650 s) and CD_2Cl_2 (470 s) is not regarded as significant.

Apparent Acid Dissociation Constants. The apparent pK_a' values for β-diketones **1**−**3** were obtained from a spectroscopically monitored acid–base titration. The term "apparent" is used in this study because no attempt was made to partition the experimentally obtained pK_a' values between the separate pK_a values of the enol and keto isomers. A solvent system of water containing 10% acetonitrile was used because, although the β-diketonates **1**$^-$−**5**$^-$ do dissolve in water at high pH, the β-diketones **1**–**5** precipitate as they form upon titration with acid. Acetonitrile was chosen as cosolvent because it has a small influence on pK_a' determinations,[14] as demonstrated by pK_a' values of a model compound, acetylacetone, in water (pK_a' = 8.83) and water containing 10% acetonitrile (pK_a' = 8.93).

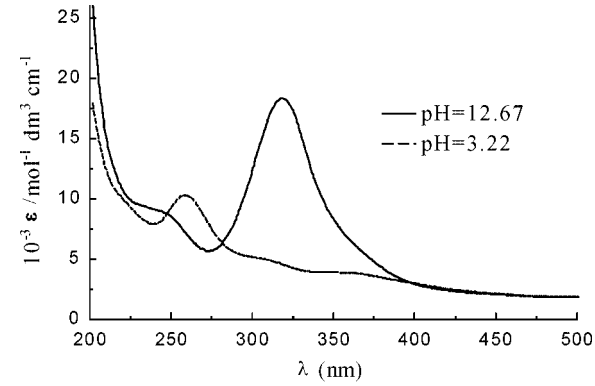

Figure 4. UV/vis spectra of **2** (- - -, at pH 3.22) and **2**$^-$ (—, at pH 12.67) at 25 °C. I = 0.100 mol dm^{-3} $NaClO_4$ in water containing 10% CH_3CN.

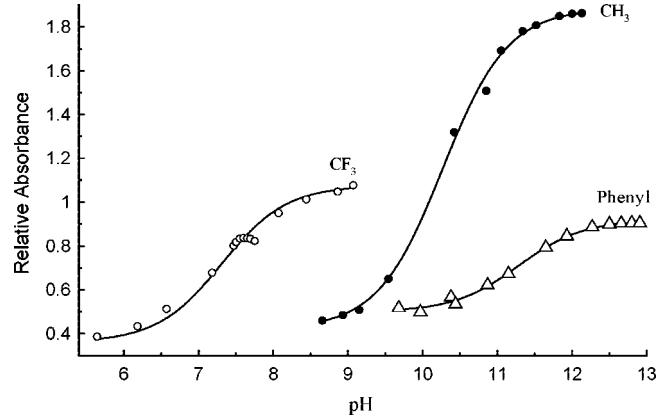

Figure 5. Relative absorbance dependence on the pH of **1** (labeled CF_3; experimental solution concentration and wavelength were 0.11 mmol dm^{-3} and 315 nm, respectively), **2** (CH_3; 0.15 mmol dm^{-3}, 319 nm) and **3** (phenyl; 0.13 mmol dm^{-3}, 365 nm) at 25 °C. I = 0.100 mol dm^{-3} $NaClO_4$ in water containing 10% CH_3CN.

Table 2. pK_a' Values Determined at λ_{exp}/nm in Water Containing 10% CH_3CN, as Well as Molar Extinction Coefficients, ϵ, in Units of dm^{3}mol^{-1}cm^{-1} at λ_{max}/nm at 25 °C[a]

compd	pK_a'	λ_{exp}	ϵ (λ_{max})[b]	λ_{max}[c]
1, χ_{CF_3} = 3.01	7.36(3)	315	5960 (260)	315
2, χ_{CH_3} = 2.34	10.22(1)	319	16890 (258)	318
3, χ_{Ph} = 2.21	11.31(4)	365	13610 (333)	347
4, χ_{Fc} = 1.87	12.9[d]	327	5840 (259)	331
5, χ_{Rc} = 1.89	12.7[e]	365	5500 (430)	339

[a] I = 0.100 mol dm^{-3} $NaClO_4$. [b] Indicated values are for the free β-diketone. [c] λ_{max} of the β-diketonato anion. [d] An average estimated value utilizing group electronegativities and cyclic voltammetric data because **4** and **5** were too acid- and base-sensitive to determine pK_a' spectrophotometrically. [e] An estimate based on group electronegativities.

Figure 4 shows the UV/vis spectra of **2** and **2**$^-$. From such spectra, a suitable wavelength was identified to follow each titration. The absorbance dependence on pH for compounds **1**−**3** can be seen in Figure 5. The new pK_a' values obtained from these S curves are summarized in Table 2. For **1** it was noted (Figure 5) that, at around the midpoint of the titration, there was an unidentified process occurring.

However, this did not noticeably affect the pK_a' value as the S curve retained its shape over the 2 unit pH range wherein a pK_a' value is determined. It is possible that this unknown process could be reversible hydroxylation, which has been previously

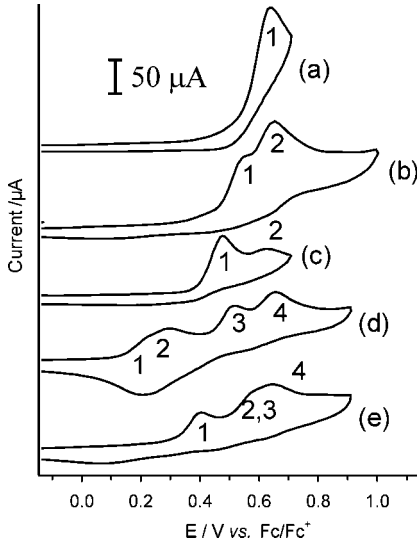

Figure 6. CVs of 2.0 mmol dm^{-3} solutions of $RcCOCH_2COR$ in CH_3CN/0.1 mol dm^{-3} $N(^nBu)_4PF_6$ utilizing a glassy-carbon electrode at a scan rate of 250 mV s^{-1}: (a) **1**, R = CF_3; (b) **2**, R = CH_3; (c) **3**, R = C_6H_5; (d) **4**, R = Fc; (e) **5**, R = Rc.

noted in other trifluoro-containing β-diketones.[24,14] β-Diketone stability in basic media are as follows: (most stable) **1** (R = CF_3) >> **2** (R = CH_3) > **3** (R = Ph) >> **4** (R = Fc) ≈ **5** (R = Rc) (least stable).

No spectroscopically determined pK_a' values could be found for **4** and **5**, because they decomposed too quickly at high pH for meaningful spectroscopic measurements. In general, though, β-diketone acid strength decreases as χ_R decreases. From ref 16, a linear dependence between pK_a' and χ_R values described by the equation p$K_a' = -6.4542\chi_R + 25$ for the analogous ferrocene series $FcCOCH_2COR$, was observed. From this equation, for **4** where R = Rc, $\chi_{Rc} = 1.89$ equates with a pK_a' value of 12.8.

To estimate the pK_a' value for **5**, another approach utilizing the sum of χ_R values for pendant R groups on β-diketones of the type $R^1COCH_2COR^2$ was used. Utilizing once again the analogous ferrocene series $FcCOCH_2COR$ of ref 16 as well as **4**, the relationship between pK_a and $(\chi_{R1} + \chi_{R^2})$ was determined as p$K_a' = -6.4954(\chi_{R^1} + \chi_{R^2}) + 37.26$. Since $\chi_{Rc} = 1.89$, an estimate of the pK_a' value of **5** is 12.7. This value is exactly the same as that obtained by inserting $\chi_{Rc} = 1.89$ into the linear trend line p$K_a' = -4.8629\chi_R + 21.91$, describing the relationship between pK_a' and χ_R values for the *present ruthenocene* series, $RcCOCH_2COR$. This result gives ample proof that, for the present class of β-diketones, it is justified to estimate pK_a' values utilizing $\chi_{R^1} + \chi_{R^2}$ values if there are no common pendant β-diketone R substituents or χ_R relationships if there is a common R substituent on the β-diketone core, $R^1COCH_2COR^2$.

Electrochemistry. Irreversible electrochemistry was found for the ruthenocenyl centers of **1**–**5** in acetonitrile at a glassy-carbon working electrode in the presence of 0.1 mol dm^{-3} $N(^nBu)_4PF_6$ supporting electrolyte. Only peak anodic potentials, $E_{p,a}$, vs Fc/Fc^+ in the potential range 0.38 V < $E_{p,a}$ < 0.67 V were observed in their cyclic voltammograms (CVs) (Figures 6 and 7). In contrast, the ferrocenyl center of **4** showed reversible electrochemistry with estimated enol and keto formal reduction potentials $E^{\circ\prime} = ½(E_{p,a} + E_{p,c}) = 0.213$ and 0.244 V vs Fc/Fc^+, respectively, upon assuming $\Delta E_p = E_{p,a} - E_{p,c} = 74$ mV, the same as that for free ferrocene, at a scan rate of 50 mV s^{-1} (Table 3, Figures 6 and 7). In comparison, we found that for ferrocene itself $\Delta E_p = 74$ mV, $i_{p,c}/i_{p,a} = 0.98$, and $E^{\circ\prime} = 0.087$ V vs Ag/Ag^+ under similar conditions. Relevant CV parameters are summarized in Table 3.

While **1** showed only one observable anodic peak, multiple ruthenocenyl oxidation peaks are observed for **2**–**5** (Table 3 and Figures 6 and 7). This is easily explained as follows: for **1**, the equilibrium keto content is only 7.5% (Table 1). This small amount, which forms at a kinetic rate having a half-life of more

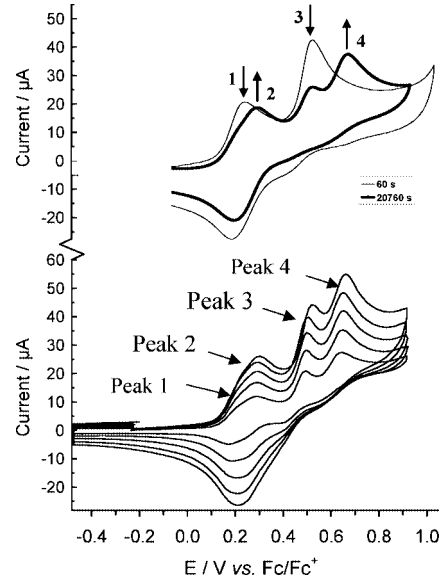

Figure 7. (Top) CVs of a 2.0 mmol dm^{-3} enol solution and of a near-equilibrium solution (bold line) of **4** in CH_3CN/0.1 mol dm^{-3} $N(^nBu)_4PF_6$ at 20 °C utilizing a glassy-carbon electrode and scan rate of 100 mV s^{-1} recorded at the indicated times after dissolving the sample. (Bottom) CVs of an equilibrium CH_3CN solution of **4** at scan rates of 50 (smallest current), 100, 150, 200, and 250 mV s^{-1}.

Table 3. Peak Anodic Potentials vs Fc/Fc^+ and Peak Anodic Currents for β-Diketones 1–5 in CH_3CN/0.1 mol dm^{-3} $N(^nBu)_4PF_6$, as Well as Data for 4 in CH_2Cl_2

compd (% enol[a])	$E_{p,a}(1)$/V	$i_{p,a}(1)/\mu$A	$E_{p,a}(2)$/V	$i_{p,a}(2)/\mu$A
1, $\chi_{CF_3} = 3.01$ (92.5)	0.609	51.3		
2, $\chi_{CH_3} = 2.34$ (68.5)	0.473	23.2	0.584	27.0
3, $\chi_{Ph} = 2.21$ (85.0)	0.451	20.3	0.605	9.2
4, $\chi_{Fc} = 1.87$ (42.5)	0.250[b] (Fc^1)	*c*	0.281[b] (Fc^2)	*c*
$\chi_{Fc^+} = 2.82$	0.484[d] (Rc^3)	20.0	0.636[d] (Rc^4)	25.8
in CH_2Cl_2,[e] (50.1)	0.265[e] (Fc^1)	*c*	0.314[e] (Fc^2)	*c*
dimer: $E_{p,c} = 0.515$[g]	0.802[f] (Rc^3)	*c*	0.883[f] (Rc^4)	
5, $\chi_{Rc} = 1.89$	0.213 (Rc^1)	9.0	0.403[h] (Rc^2)	*c*
	0.403[h] (Rc^3)	*c*	0.480 (Rc^4)	20.8

[a] By ^1H NMR in $CDCl_3$ at equilibrium. [b] Due to poor peak resolution, $E_{p,a}(1)$ could not be measured; $E_{p,c} = 0.176$ V. Upon assuming $\Delta E_p = 74$ mV, as was found for free ferrocene under our conditions, $E_{p,a}$ could be estimated, and formal reduction potential estimates are $E^{\circ\prime}{}_1 \approx 0.213$ and $E^{\circ\prime}{}_2 \approx 0.244$ V vs Fc/Fc^+. [c] Poor peak resolution disallowed peak current measurement. [d] $E_{p,a}(3)$, the ruthenocenyl oxidation potential of the enol form, and $E_{p,a}(4)$, that of the keto form, of **4** after the ferrocenyl group has *already* been oxidized to ferrocenium. [e] In CH_2Cl_2/0.1 M $[N(^nBu)_4][B(C_6F_5)_4]$. $E^{\circ\prime}{}_1$(enol) and $E^{\circ\prime}{}_2$(keto) are estimated at 0.210 and 0.258 V respectively (see the Supporting Information). ΔE values in CH_2Cl_2 are slightly larger than in CH_3CN. [f] Ruthenocenyl oxidation potentials in CH_2Cl_2/0.1 M $[N(^nBu)_4][B(C_6F_5)_4]$ of the enol and keto forms of **4**. [g] In CH_2Cl_2, a weak reduction potential was observed which is consistent with dimerization of a Ru^{III} species, in analogy with what was found for free ruthenocene. [h] The provided E_p value is the observed peak potential for the overlaid (combined) peaks 2 and 3 of **5**.

(24) (a) Aygen, S.; van Eldik, R. *Chem. Ber.* **1989**, *122*, 315. (b) Ellinger, M.; Duschner, H.; Starke, K *J. Inorg. Nucl. Chem.* **1978**, *40*, 1063.

than 8 h from freshly prepared enol-enriched solutions, will be very difficult to detect. The large $i_{p,a}(1)$ value reported in Table 3 for **1**, compared with those of **2**–**5**, is therefore indicative of a large enol content at the time of measurement. In contrast, the peak pairs for **2**−**5** are consistent with the existence of keto and enol isomers in solution at the time of measurement. The equilibrium keto content of **2**−**5** varies between 15 and 53% (Table 1). From the CV of **3** (Figure 6) it was concluded that the smaller CV peak, peak 2, belongs to the keto isomer because the keto content at equilibrium for **3** is much less than the enol content. By analogy, peak 2 for **2** and peaks 2 and 4 for **4** and **5** are also assigned to the keto isomers. To prove the keto and enol peak assignments as correct, CVs were recorded of aged samples of each compound. These samples are enol-enriched, and the keto peaks were found to be either absent or much less pronounced, depending on how quickly after the sample dissolved the CVs were recorded. Figure 7 demonstrates this for **4**.

For the symmetrical β-diketone **5**, peaks 2 and 3 were overlapping (Figure 6). Different formal reduction potentials for side groups on symmetrical complexes in which mixed-valent intermediates are generated are well-known in systems that allow electron delocalization, either through bridge-mediated paths or from a direct metal−metal interaction.[16,25] This then implies that, for **5**, overlapping peaks 2 and 3 represent the oxidation of the keto isomer $Rc^3COCH_2CORc^4$ and the oxidation of the mixed-valent enol intermediate $Rc^{1,ox}C(OH)=CHCORc^2$, respectively. By necessity, peak 1 can only involve $Rc^1C(OH)=CHCORc^2$ oxidation and peak 4 must involve $Rc^{1,ox}COCH_2CORc^2$ oxidation. Equation 4 highlights the electrochemical oxidation of enol and keto oxidation as well as the slow chemical equilibrium that exists between the different enol and keto forms.

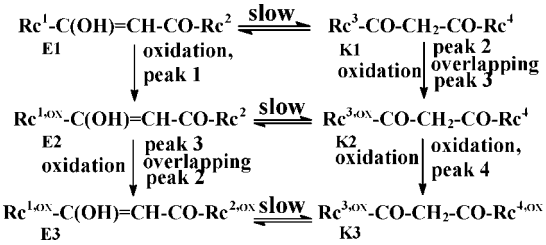

(4)

The oxidized species E2 is not considered to be $Rc^1C(OH)=CHCORc^{2,ox}$, because carbonyl (C=O) substituted metallocenes are oxidized at potentials greater (more positive) than those for alcohol (OH) substituted metallocenes.[25e] Bulk electrolyses to determine the ruthenium oxidation state in Rc^{ox} above failed due to compound decomposition, but it is generally accepted that Ru^{IV} species arise in CV experiments involving ruthenocene derivatives[19,20] in $CH_3CN/N(^nBu)_4PF_6$ media. From previous research,[26] a Ru^{IV} species such as $[(C_5H_4R)(Cp)Ru^{IV}CH_3CN]^{2+}$ is very likely formed in the present electrochemistry study in CH_3CN. However, Mann[20] and, more recently, Geiger[27] reported reversible Rc oxidation to two Ru^{III} species, one monomeric $[(C_5H_5)_2Ru^{III}]^+$ and the other dimeric $[(C_5H_5)_2Ru^{III}Ru^{III}(C_5H_5)_2]^{2+}$, in a $CH_2Cl_2/[N(^nBu)_4][B\{(C_6H_3)(CF_3)_2\}_4]$ or $CH_2Cl_2/[N(^nBu)_4][B(C_6F_5)_4]$ medium, respectively. It was also noted in the ^1H NMR kinetic study (Table 1) that more electron-withdrawing R substituents shift the keto–enol equilibrium position to the enol side. This implies the equilibrium positions of the E2/K2 and E3/K3 equilibria in eq 4 lies to the left of that for the E1/K1 equilibrium. This will be so because $Rc^{i,ox}$, $i = 1$–4, like the ferrocenium cation, Fc^+,[16] is more electron-withdrawing than the Rc group itself.

From the above it is clear that ruthenocenyl $E_{p,a}$ potentials must be dependent on χ_R. In Table 3 it can be seen that $E_{p,a}(1)$, the anodic ruthenocenyl oxidation potential of the enol isomer of **1**−**3** and **5**, becomes smaller as χ_R decreases. In contrast, for **4**, the corresponding ruthenocenyl oxidation wave is $E_{p,a}(3)$, but the potential at which this wave is found has the second largest value in the present compound series, despite the fact that the ferrocenyl group has the lowest χ_R value of all R substituents. However, for **4**, the ferrocenyl group is first oxidized to ferrocenium during CV scans. Hence, when the first ruthenocenyl wave (the wave for the enol isomer) is observed at $E_{p,a}(3) = 484$ mV vs Fc/Fc^+, the group electronegativity of the ferrocenium species,[16] $\chi_{Fc^+} = 2.82$, is relevant. This is also the second largest χ_R value in the present compound series. Thus, **4** follows the general χ_R dependence for ruthenocenyl oxidation as well.

No electrochemical estimate of the pK_a' value of **5** could be made, since the ruthenocenyl center does not represent a thermodynamic reversible redox center and no simple linear relationship between $E_{p,a}(Rc)$ and pK_a' could be found (see the Supporting Information).

Isomerization Kinetics Utilizing Electrochemical Measurements. (a) CH_3CN as Solvent. The good resolution between keto and enol peaks of Figure 7 suggests it must in principle be possible to follow the kinetics of isomerization for **2**−**5** electrochemically, because they all have a large difference in keto content at equilibrium, and because the peak current, i_p, is directly proportional to concentration, C, according to the Randles−Sevcik equation: $i_p = (2.69 \times 10^5)n^{3/2}AD^{1/2}C\nu^{1/2}$.[28] Several problems are associated with CV and OYSW measurements that normally would disqualify these techniques as useful methods in kinetic studies. The most serious of these is electrode fouling (polluting) that may occur during the extended periods of time required for slow kinetic changes. For **4**, electrode fouling led to the following: (i)a loss of peak resolution especially for waves 1 and 2, (ii) a ruthenocenyl-based $E_{p,a}$ potential drift of more than 120 mV to more positive values, and (iii) a slow systematic decrease in current intensity as the electrode surface was compromised.

These problems were overcome by replacing measured i_p values with percent keto content relative to an internal standard, free ferrocene, as described in the Experimental Section. Thus, time-based CV experiments on **4** led to rate constants that only scattered in the range (8–14) $\times 10^{-5}$ s^{-1}. These CV-determined rate constants are mutually consistent with the ^1H NMR determined rate constant of 9.1×10^{-5} s^{-1} (Table 1). Examples of time-based CV scans and the workup procedure to obtain rate constants in CH_3CN solutions are available as Supporting Information; the next section describes examples for CH_2Cl_2

(25) Leading references are: (a) Creutz, C.; Taube, H. *J. Am. Chem. Soc.* **1969**, *91*, 3988. (b) Geiger, W. E.; van Order, N.; Pierce, D. T.; Bitterwolf, T. E.; Rheingold, A. L.; Chasteen, N. D. *Organometallics* **1991**, *10*, 2403. (c) van Order, N.; Geiger, W. E.; Bitterwolf, T. E.; Rheingold, A. L. *J. Am. Chem. Soc.* **1987**, *109*, 5680. (d) Pierce, D. T.; Geiger, W. E. *Inorg. Chem.* **1994**, *33*, 373. (e) Davis, W. L.; Shago, R. F.; Langner, E. H. G.; Swarts, J. C. *Polyhedron* **2005**, *24*, 1611.

(26) (a) Watanaba, M.; Motoyama, I.; Takayama, T.; Sato, M. *J. Organomet. Chem.* **1997**, *549*, 13. (b) Watanaba, M.; Motoyama, I.; Shimoi, M.; Sano, H. *J. Organomet. Chem.* **1996**, *517*, 115. (c) Smith, T. P.; Iverson, D. J.; Droege, M. W.; Kwan, K. S.; Taube, H. *Inorg. Chem.* **1987**, *26*, 2882.

(27) Trupia, S.; Nafady, A.; Geiger, W. E. *Inorg. Chem.* **2003**, *42*, 5480.

(28) Kissinger, P. T.; Heineman, W. R. In *Laboratory Techniques in Electroanalytical Chemistry*; Marcel Dekker: New York, 1984; p 82.

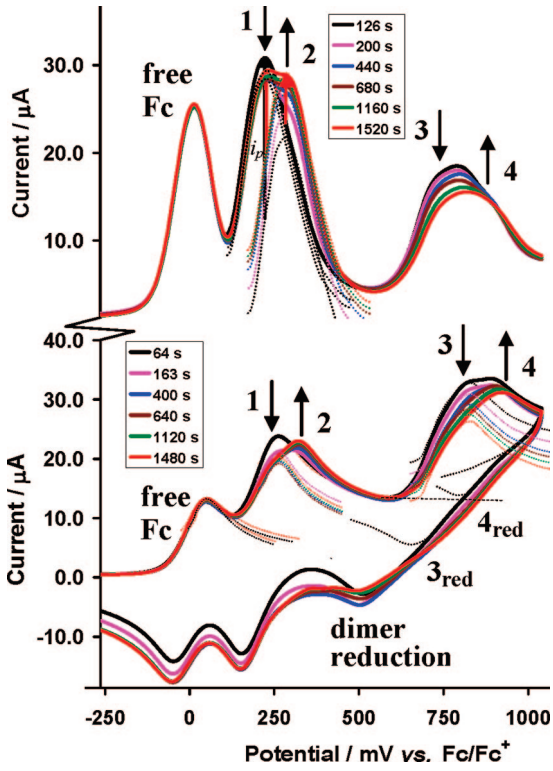

Figure 8. Sample Osteryoung square wave voltammograms (top, at 50 Hz) and cyclic voltammograms (bottom, at scan rate 200 mV s^{-1}) in CH_2Cl_2 at 20 °C, showing how the enol form (peaks 1 and 3) becomes less prominent while the keto form becomes more prominent (peaks 2 and 4) as an enol-enriched solution of **4** approaches equilibrium. For the CV, dotted lines show anticipated decay curves. For the OYSW voltammograms, the dotted lines show the peaks of waves 1 and 2 independent of the influence of each other. This allowed measurement of i_p as described in the text and Supporting Information.

solutions. Poor peak resolution between peaks 1 and 2 disallowed following of this reaction utilizing the ferrocenyl wave of **4**. Attempts to follow the kinetics in CH_3CN with Osteryoung square wave voltammetry were unsuccessful.

(b) CH_2Cl_2 as Solvent. In an attempt to prove the existence of a $[(C_5H_5)Ru^{III}(C_5H_4R)]^+/[(C_5H_5)Ru^{II}(C_5H_4R)]$ couple during the electrochemical investigation of the present β-diketone series, the electrochemical kinetics of **4** were reinvestigated in a noncoordinative CH_2Cl_2/0.1 mol dm^{-3} $[N(^nBu)_4][B(C_6F_5)_4]$ solvent/supporting electrolyte system following the guidelines of Geiger.[27] In addition, from ^1H NMR measurements, isomerization kinetics in CH_2Cl_2 is almost 20 times faster than in CH_3CN, which gives less time for electrode pollution. In CH_2Cl_2, the resolutions of ferrocenyl waves 1 and 2 were markedly improved, especially in the presence of free ferrocene as internal standard. However, the two ruthenocenyl waves at peaks 3 ($E_{p,a}$ = 0.802 V) and 4 ($E_{p,a}$ = 0.883 V) became much *less* resolved than was the case in CH_3CN. Clear evidence of a $[(C_5H_5)Ru^{III}(C_5H_4R)]^+$ species was also found, since a cathodic current for the ruthenocenyl group during the reverse sweep could clearly be seen, (Figure 8 and the Supporting Information).

When potentials are not referenced against the experimentally used Ag/Ag^+ reference electrode, but rather versus an internal standard, here Fc/Fc^+, as first suggested by Gagny,[29] direct potential comparisons between the CH_3CN and CH_2Cl_2 solvent systems become possible (see Supporting Information for a treatment of potential data versus both the experimentally used Ag/Ag^+ reference electrode and versus Fc/Fc^+ as internal standard). The key result from this treatment is that, although formal reduction potentials versus Fc/Fc^+ for ferrocenyl-based waves 1 and 2 of **4** are for all practical purposes the same in both solvents, potentials associated with ruthenocenyl waves 3 and 4 of **4** were shifted to much more positive potentials in CH_2Cl_2 (Table 3). Different ruthenocene oxidation products appear to form in CH_3CN and CH_2Cl_2. The ruthenocenyl fragment oxidation product in CH_3CN is probably the Ru^{IV} species $[(C_5H_4R)(Cp)Ru^{IV}\cdot CH_3CN]^{2+}$, while in CH_2Cl_2, the labile Ru^{III} species $[(C_5H_5)Ru^{III}(C_5H_4R)]^+$ is first formed during oxidation. In contrast with this, in both solvents ferrocene oxidation only gave the Fe^{III} species $[(C_5H_5)Fe^{III}(C_5H_4R)]^+$. These results highlight different substrate−solvent interactions (CH_3CN in contrast with CH_2Cl_2). In particular it shows that strong CH_3CN association occurs with the *oxidized ruthenocenyl fragment* of **4** but that CH_3CN association with the *oxidized ferrocenyl fragment of the same molecule* are so weak that for all practical purposes, it can be neglected.

The $i_{p,c}/i_{p,a}$ current ratio for waves 3 and 4 deviate substantially from unity in CH_2Cl_2. The results, therefore, are consistent with unstable, i.e. quickly decomposing $(C_5H_5)Ru^{III}(C_5H_4R)$ fragments forming during the oxidation of the ruthenocenyl group of **4** at 20 °C. The position of the most prominent $(C_5H_5)Ru^{III}(C_5H_4R)$ fragment reduction wave at E = ca. 0.515 V vs Fc/Fc^+ at 20 °C in CH_2Cl_2 (Figure 8) is consistent with a two-electron Ru^{III} dimer reduction in analogy to free ruthenocene,[27] because it is found at a potential ca. 290 mV lower than $E_{p,a}$(peak 3) = 802 mV. This peak potential difference is too large to be associated with a simple $(C_5H_5)Ru^{III}(C_5H_4R)]^+/[(C_5H_5)Ru^{II}(C_5H_4R)$ couple. However, weak peak shoulders 3_{red} and 4_{red} are observed at $E_{cathodic}$ = ca. 671 and 777 mV, respectively (Figure 8 and, more clearly, the Supporting Information). A repeat CV experiment in CH_2Cl_2 performed not at 20 °C but at 0 °C revealed a reduction peak associated with wave 3 at 662 mV vs Fc/Fc^+ but no dimer reduction peak at ca. 515 mV vs Fc/Fc^+ (see the Supporting Information). Despite the weakness of shoulders 3_{red} and 4_{red} that obviously hampers Ru^{III} reduction peak assignments, key information can be extracted from them. The estimated $\Delta E_p = E_{p,a}$(peak i) − $E_{p,c}$(shoulder i) values of ca. 131 and 106 mV for peak/shoulder pairs 3 and 4 allow them to be associated with reversible to quasi-reversible one-electron-transfer processes. They are consistent with simple $(C_5H_5)Ru^{III}(C_5H_4R)]^+/[(C_5H_5)Ru^{II}(C_5H_4R)$ couples. Utilizing the above CH_2Cl_2 results, eq 4 can be amended for compound **4** to involve electrochemical reversible one-electron oxidation during the generation of E2, K2, E3, and K3. Then, $Rc^1/Rc^{1,ox}$ and $Rc^3/Rc^{3,ox}$ will be the $Fe^{II/III}$ fragments $(C_5H_5)Fe^{II/III}(C_5H_4R)$, while $Rc^{2,ox}$ and $Rc^{4,ox}$ will be $[(C_5H_5)Ru^{III}(C_5H_4R)]^+$. Provision must also be made for a two-electron reduction of at least one Ru^{III} dimer back to the ruthenocenyl group. With the present knowledge, the dimer is most likely $[(C_5H_4R)(C_5H_5)Ru^{III}-Ru^{III}(C_5H_5)(C_5H_4R)]^{2+}$, another form of a $Ru^{III}-Ru^{III}$ dimer in analogy with ruthenocene[27] itself, or one of the two possible dimers that was found for the analogous osmocene[30] system.

Table 4 summarizes sets of data utilized to obtain isomerization rate constants from three different electrochemical sets of kinetic experiments performed in CH_2Cl_2. Time-based plots

(29) Gagne, R. R.; Koval, C. A.; Lisensky, G. C. *Inorg. Chem.* **1980**, *19*, 2855.

(30) Droege, M. W.; Harman, W. D.; Taube, H. *Inorg. Chem.* **1987**, *26*, 1309.

Table 4. Cyclic Voltammetry Data of Ferrocenyl Waves 1 and 2 (labeled as Fc-CV) and Ruthenocenyl Waves 3 and 4 (Rc-CV) Collected with Time for the Conversion of Enol to Keto Isomers of $RcCOCH_2COFc$ in CH_2Cl_2 at 20 °C[a]

	Fc CV/Rc CV (Fc SW)			
measmt time/s	$i_{p,a}$(enol)/μA	$i_{p,a}$ (keto)/μA	% keto[b]	$\ln((\%\ \text{keto})_0 - (\%\ \text{keto})_\infty)/((\%\ \text{keto})_t - (\%\ \text{keto})\infty)$
0/0 (0)	−[c]/−[c] (−)[c]	−[c]/−[c] (−)[c]	0[d]/0[d] (0)[d]	0[d]/0[d] (0)[d]
64/64 (200)	41.5/49 (44)	3/6.7 (14)	6.7/12.0 (24.1)	0.183/0.288 (0.702)
163/163 (440)	38/43 (34)	8.2/11 (19)	17.7/20.4 (35.9)	0.584/0.616 (1.391)
400/400 (680)	34/40 (31)	14/17 (22)	29.1/29.8 (41.5)	1.300/1.236 (2.027)
640/640 (1160)	32/36 (30)	16/21 (24)	33.3/36.8 (46.7)	1.787/2.089 (3.712)
1120/1120 (1520)	29/34 (29)	18/23.4 (27)	38.3/40.8 (48.2)	3.158/3.555 (−)[e]
$t = \infty$	−[c]/−[c] (−)[c]	−[c]/−[c] (−)[c]	40[d]/42[d] (47.8)[d]	

[a] Values in parentheses correspond to Osteryoung square wave data of ferrocenyl waves 1 and 2 (Fc-SW). [b] % keto = $i_{p,a}$(keto)/($i_{p,a}$(keto) + $i_{p,a}$(enol)) × 100. [c] Not measured due to the time required for dissolving analytes. [d] Values not measured but obtained from a nonlinear least-squares MINSQ fit. [e] Because the measured i_p value is larger than the calculated t_∞ value, this data point was not calculated.

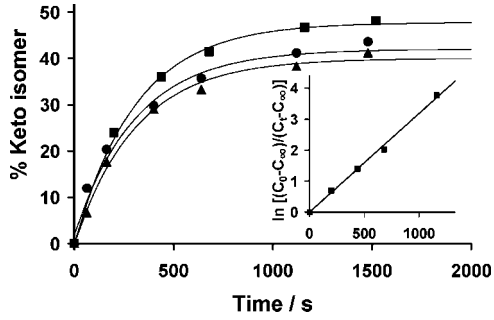

Figure 9. Time traces showing the formation of percent keto isomer as determined by ferrocenyl-based Osteryoung square wave (■, top), ruthenocenyl-based cyclic (●, middle) ,and ferrocenyl-based cyclic (▲, bottom) voltammetry for **4** at 25 °C in CH_2Cl_2. Insert: kinetic plot of ferrocenyl-based Osteryoung square wave data from Table 4 for this isomerization. The slope of this graph gives the first-order rate constant $k_{obsd} = k_1 + k_{-1} = 0.0031\ s^{-1}$ (C = percent keto isomer).

showing how the percent keto isomer increases as the equilibrium position is approached from the enol side for all three electrochemical experimental approaches are shown in Figure 9. The insert highlights the validity of a first-order treatment of ferrocenyl-based Osteryoung square wave obtained kinetic data. Rate constants $k_{obsd} = k_1 + k_{-1}$ for all three techniques approached $3 \times 10^{-3}\ s^{-1}$ and deviated only by a factor of about 2 from the ^1H NMR determined rate constant of $1.47 \times 10^{-3}\ s^{-1}$ (Table 1). These spectroscopic and electrochemical equivalent kinetic results are in extraordinary good agreement if one bears in mind all the current measurement difficulties associated with electrode fouling over extended periods of time.

Finally, the percent keto isomer values at equilibrium in CH_2Cl_2 as obtained by the Fc-CV, Rc-CV and Fc-OYSW experiments are 40, 42, and 47.8%, respectively (Table 4). These values are in fair to good agreement with the ^1H NMR determined value of 50.1−50.2%. The ^1H NMR determined equilibrium constant K_c = 1.00–1.01 is in equally good agreement with the values determined by Fc-CV (1.50), Rc-CV (1.38), and Fc-OYSW (1.09) measurements (Table 1).

Conclusion

A series of ruthenocene-containing β-diketones of the form $RcCOCH_2COR$ with R = CF_3, CH_3, Ph, Fc, Rc were synthesized and characterized, and pK_a' values were determined. Although all β-diketones converted quantitatively with time in the solid state to one enol form, in solution these ligands exist in a dynamic equilibrium as a mixture of keto and enol isomers. Rate constants of these interconversions, as well as the corresponding equilibrium constants, were determined utilizing ^1H NMR spectroscopy, cyclic voltammetry, or Osteryoung square wave voltammetry. In contrast to the case for the ferrocenyl group, the ruthenocenyl fragment exhibited irreversible electrochemistry in CH_3CN/0.1 mol dm^{-3} $N(^nBu)_4PF_6$. Only oxidation waves generating most likely a Ru^{IV} oxidized product could be detected. In CH_2Cl_2/0.1 mol dm^{-3} $[N(^nBu)_4][B(C_6F_5)_4]$, however, clear evidence for the electrochemical reversible generation of unstable $[(C_5H_5)Ru^{III}(C_5H_4R)]^+$ and a dimerized oxidized product was found. Kinetic measurement utilizing cyclic voltammetry and/or Osteryoung square wave techniques is possible, provided extensive care is taken in estimating decay currents. Excessively long kinetic experiments are more difficult to follow electrochemically, especially because of electrode fouling. The accuracy of the electrochemical technique in studying solution reaction kinetics is on a par with that of spectroscopic techniques. Isomerization kinetics, equilibrium constants, pK_a' values, and ruthenocenyl oxidation potentials were shown to be dependent on the group electronegativity of the R side group in $RcCOCH_2COR$. These new ligands will open up research in new multinuclear metal coordination complexes with interesting properties.

Experimental Section

General Information. Ruthenocene (Strem) and aluminum trichloride and other solid reagents (Aldrich) were used without further purification. Dry acetonitrile was obtained by reflux under nitrogen over calcium hydride, distillation onto alumina for storage, and redistillation just prior to use. THF was dried by reflux under a nitrogen atmosphere over sodium wire and distillation directly before use. Water was double-distilled. Acetylruthenocene (**2**) was synthesized as described before, utilizing 2.2 mol equiv[31] of $AlCl_3$. Methyl ferrocenoate was prepared by following published guidelines,[14] and this method was directly adapted for methyl ruthenocenoate. Chromatography was performed on Kieselgel 60 (Merck, grain size 0.063–0.2 mm) utilizing 1:1 ether−hexane by volume as eluant unless otherwise indicated. ^1H NMR spectra at 20 °C were recorded on a Bruker Advance DPX 300 NMR spectrometer at 300 MHz, with chemical shifts presented as δ values referenced to $SiMe_4$ at 0.00 ppm utilizing $CDCl_3$ as solvent. The $CDCl_3$ was made acid-free by passing it through basic alumina immediately before use. Elemental analysis was conducted by the Canadian Microanalytical Service, Ltd.

***β*-Diketone Syntheses.** The syntheses of **1** may serve as an example. To a solution of acetylruthenocene (0.799 g; 2.922 mmol) in dry THF (5 mL) was added lithium diisopropylamide (1.46 cm^3 of 2.0 mol dm^{-3} solution; 2.92 mmol), and the reaction mixture was stirred for 20 min while it was cooled on ice. Ethyl trifluoroacetate (0.42 g; 0.35 cm^3; 2.921 mmol) was added and the

(31) Rausch, M. D.; Fischer, E. O.; Grubert, H. *J. Am. Chem. Soc.* **1960**, *82*, 76.

reaction mixture stirred for 16 h at room temperature before an excess of ether (>30 cm^3) was added. The precipitate was filtered off, added to an ice-cold HCl solution (0.1 mol dm^{-3}; 100 cm^3), and stirred for 5 min and the product extracted into ether. The ether layer was washed with H_2O (3 × 100 cm^3), dried over $MgSO_4$, filtered, and evaporated to dryness under reduced pressure. The crude product was purified using column chromatography with 4:1 ether−hexane by volume as eluent (R_f = 0.91). Yield: 83%. Mp: 102–104 °C. ^{1}H NMR (300 MHz, $CDCl_3$; δ_H): enol isomer (92.5% at equilibrium), 6.03 (1H; s; COC<u>H</u>CO), 5.20 (2H; t; C_5H_4), 4.93 (2H enol overlapping with keto signal; t; C_5H_4), 4.63 (5H; s; C_5H_5); keto isomer (7.5%), 5.12 (2H; t; C_5H_4), 4.93 (2H, keto overlapping with enol signal; t; C_5H_4), 4.70 (5H; s; C_5H_5), 3.00 (2H; s; $COCH_2CO$). Anal. Calcd for $C_{14}F_3H_{11}O_2Ru$: C, 45.51; H, 3.00. Found: C, 45.50; H, 3.00.

Characterization Data for 2–5. Compound 2. The product was purified using column chromatography (R_f = 0.66). Yield: 26.8%. Mp: 111 °C. ^{1}H NMR (300 MHz; $CDCl_3$; δ_H): enol isomer (68.5%), 5.64 (1H; s; COC*H*CO), 5.11 (2H; t; C_5H_4), 4.79 (2H enol overlapping with keto signal; t; C_5H_4), 4.59 (5H; s; C_5H_5), 2.31 (3H; d; CH_3); % keto (31.5%), 5.14 (2H; t; C_5H_4), 4.79 (2H keto overlapping with enol signal; t; C_5H_4), 4.61 (5H; s; C_5H_5), 3.73 (2H; s; $COCH_2CO$), 2.05 (3H; d; CH_3). Anal. Calcd for $C_{14}H_{14}O_2Ru$: C, 53.30; H, 4.47. Found: C, 53.63; H, 4.75.

Compound 3. The product was difficult to purify using column chromatography with 2:1 ether−hexane as eluent (R_f = 0.66); crystallization as for **4** worked better. Yield: 41.3%. Mp: 110 °C. ^{1}H NMR (300 MHz; $CDCl_3$; δ_H): enol (85.00%), 7.85 (2H; m; C_6H_5), 7.46 (3H; m; C_6H_5), 6.28 (1H; s; COCHCO), 5.25 (2H; t; C_5H_4), 4.83 (2H enol overlapping with keto signal; t; C_5H_4), 4.59 (5H; s; C_5H_5); keto (15.0%), 8.1 (2H; m; C_6H_5), 7.60 (3H; m; C_6H_5), 5.18 (2H; t; C_5H_4), 4.83 (2H keto overlapping with enol signal; t; C_5H_4), 4.48 (5H; s; C_5H_5), 4.25 (2H; s; $COCH_2CO$). Anal. Calcd for $C_{19}H_{16}O_2Ru$: C, 60.45; H, 4.27. Found: C, 60.38; H, 4.38.

Compound 4. Purification was by crystallization from 1:1 heptane−chloroform and allowing the chloroform to slowly evaporate. Yield: 34%. Mp: 178 °C. ^{1}H NMR (300 MHz; $CDCl_3$; δ_H): enol to the Fc side (47.0%), 5.9 (1H; s; COCHCO), 5.19 (2H; t; C_5H_4 Rc), 4.81 (2H + 2H Rc enol overlapping with Fc enol signal; t; C_5H_4), 4.60 (5H; s; C_5H_5 Rc), 4.51 (2H; t; C_5H_4 Fc), 4.20 (5H; s; C_5H_5 Fc); enol to Rc side (14.0%), 6.60 (1H; s; COCHCO), 5.14 (2H; t; C_5H_4 Rc), 4.81 (2H + 2H Rc enol overlapping with Fc enol signal; t; C_5H_4), 4.72 (2H; t; C_5H_4 Fc), 4.56 (5H; s; C_5H_5 Rc), 3.99 (5H; s; C_5H_5 Fc); keto (39.0%), 5.24 (2H; t; C_5H_4 Rc), 5.10 (2H; t; C_5H_4 Fc), 4.94 (2H + 2H Rc keto overlapping with Fc keto signal; t; C_5H_4 Rc), 4.61 (5H; s; C_5H_5 Rc), 4.23 (5H; s; C_5H_5 Fc), 2.28 (2H; s; $COCH_2CO$). Anal. Calcd for $C_{23}FeH_{20}O_2Ru$: C, 56.77; H, 4.14. Found: C, 56.80; H, 4.16.

Compound 5. The product was purified using column chromatography (R_f = 0.66). Yield: 28%. Mp: 182 °C. ^{1}H NMR (300 MHz; $CDCl_3$; δ_H): enol (41.2%), 5.83 (1H; s; COC*H*CO), 5.17 (2H; t; C_5H_4), 4.84 (5H; s; C_5H_5), 4.78 (2H; t; C_5H_4); keto (58.8%), 5.23 (2H; t; C_5H_4), 4.83 (2H; t; C_5H_4), 4.81 (5H; s; C_5H_5), 3.88 (2H; s; $COCH_2CO$), Anal. Calcd for $C_{23}H_{20}O_2Ru_2$: C, 51.96; H, 3.79. Found: C, 53.29; H, 4.08.

Percent Keto Isomer. (a) From ^{1}H NMR Spectroscopy. The percentage keto isomer at equilibrium was determined from eq 5 utilizing integral values, *I*, of the ^{1}H NMR keto/enol signal pair(s) identified in Table 1. Where more than one nonoverlapping keto/enol signal pair could be identified, the average percent keto isomer was determined. Integration of the spectra was performed such that the methine proton, RcCOC*H*═C(OH)R, at 5.5−6.5 ppm was usually assigned an integral value of 1.

$$\%\ \text{keto isomer} = \frac{I\ \text{of keto signal}}{I\ \text{of keto signal} + I\ \text{of enol signals}} \times 100 \tag{5}$$

(b) From Electrochemical Measurements. When electrochemical experiments were conducted, integral values, *I*, were replaced by peak current values, i_p, in eq 5 above to calculate the percent keto isomer.

Keto–Enol Equilibrium Constants, K_c. Once the percent keto isomer was known, the equilibrium constant, K_c, relating to eq 2 could be determined utilizing eq 6.

$$K_c = \frac{\%\ \text{enol isomer(s)}}{\%\ \text{keto isomer}} = \frac{100 - \%\ \text{keto isomer}}{\%\ \text{keto isomer}} \tag{6}$$

Isomerization Kinetics. For conversions from enol to keto isomers, solid β-diketone samples (5.5–9.6 mg/cm^{-3} $CDCl_3$) older than 3 months were quickly dissolved and ^{1}H NMR spectra recorded at appropriate times at 293 K until no further changes in the integral values of signals were observed. At this stage an equilibrium set in. The percentage keto isomer at each time interval was determined from eq 5 utilizing the same ^{1}H NMR keto/enol signal pairs identified before (Table 1). From the time-based keto percentage data fitted to eq 7,[32] the observed rate constant k_{obsd} could be calculated. The percentage keto isomer at infinite time is that of K_c, while k_1 and k_{-1} relate to equilibrium (2).

$$\ln\left[\frac{(\text{initial \% keto isomer}) - (\%\ \text{keto isomer at infinite time})}{(\%\ \text{keto isomer at time } t) - (\%\ \text{keto isomer at infinite time})}\right] = (k_1 + k_{-1})t = k_{obsd}t \tag{7}$$

The individual rate constants k_1 and k_{-1} were obtained by simultaneously solving the equations $K_c = k_1/k_{-1}$ and $k_{obsd} = k_1 + k_{-1}$. Compounds **2**−**5** were studied in this manner. Hrctfa (**1**), however, could only be studied by following the rate of conversion from keto to enol isomer. Keto-enriched solutions of **1** in sufficient concentrations for a ^{1}H NMR study were obtained by extracting a 10 cm^3 1:1 acetonitrile−ether solution (50 mg β-diketone in 10 cm^{-3}) with 5 cm^3 of 0.1 mol dm^{-3} aqueous NaOH. The aqueous layer was separated, washed with $CHCl_3$, and again separated before 2.5 cm^3 of $CDCl_3$ was added. Acidification with ice-cold 0.2 mol dm^{-3} HCl allowed extraction of the β-diketone with large keto isomer content into the $CDCl_3$ layer. The aqueous layer was discarded and the $CDCl_3$ layer quickly rinsed with water before ^{1}H NMR spectra were recorded at appropriate time intervals until the equilibrium position was reached.

Apparent Acid Dissociation Constants. pK_a' values were determined by measuring the absorbance on a Varian Cary 50 UV/vis dual beam spectrophotometer at different pH values during an acid–base titration in water or acetonitrile−water mixtures, 1:9 by volume, *I* = 0.100 mol dm^{-3} ($NaClO_4$) at 298 K at wavelengths and β-diketone concentrations as indicated in Figure 5. The wavelengths at which the absorbance dependence on pH was monitored was established by recording a UV/vis spectra for each compound at low and high pH. The chosen wavelength for the pH titration was where these two spectra exhibited meaningful different molar extinction coefficients. These spectra are shown for **2** in Figure 4. Titrations were performed with $HClO_4$ from high to low pH and then back again. β-Diketone solutions were prepared by first dissolving the compound in acetonitrile followed by dilution with the correct volume of aqueous NaOH at a convenient initial

(32) House, J. E. In *Principles of Chemical Kinetics*; W. C. Brown: Dubuque, IA, 1997; pp 46–51.

(33) Wikins, R. G. In *The Study of Kinetics and Mechanism of Reactions of Transition Metal Complexes*; Allyn and Bacon: Boston, MA, 1974; pp 44–45.

pH. pK_a' values were obtained from a least-squares fit of UV absorbance/pH data to eq 8[14,33] utilizing the fitting program MINSQ.[34]

$$A_T = \frac{A_{HA}10^{-pH} + A_A 10^{-pK_a'}}{10^{-pH} + 10^{-pK_a'}} \quad (8)$$

In eq 8, A_T = total absorbance, A_{HA} = the absorbance of the β-diketone, and A_A = the absorbance of the β-diketonate. A linear response by the pH meter (Orion Model SA 720), fitted with a glass electrode, was ensured by calibration with IUPAC standard buffers[35] at pH = $-\log \alpha_H = 4.01$, 7.00, and 12.00, respectively; α_H = activity of H^+. A test pK_a' determination was performed by titrating the well-characterized compound acetylacetone in water. The obtained pK_a' value of 8.83 ± 0.01 was, within experimental error, the same as the best available published pK_a' value for acetylacetone in water (8.878 ± 0.005 when I = 1 mol dm^{-3} and 8.98 when I = 0.0172 mol dm^{-3}).[36] It was concluded that the electrode was calibrated to measure hydrogen ion concentration under the conditions used.

Electrochemistry. Cyclic voltammetry and Osteryoung square wave voltammetry were conducted using a computer-controlled BAS Model CV-27 or BAS Model 100 B/G voltammograph. The temperature was controlled using a water bath at 20.0 ± 0.1 °C. Experiments were performed under argon on 2 mmol dm^{-3} solutions in dried distilled acetonitrile in the presence of 0.1 mol dm^{-3} [N(^{n}Bu)$_4$][PF$_6$] as supporting electrolyte or in CH_2Cl_2 in the presence of 0.1 mol dm^{-3} [N(^{n}Bu)$_4$][B(C$_6$F$_5$)$_4$].[37] The three-electrode cell that was used consisted of a glassy-carbon working electrode, with surface area 7.07 mm^2 pretreated by polishing on a Buehler microcloth first with 1 μm and then ¼ μm diamond paste, a Pt-wire counter electrode, and a reference electrode constructed from a silver wire inserted into a solution of 0.01 mol dm^{-3} $AgNO_3$ and 0.1 mol dm^{-3} tetra-*n*-butylammonium hexafluorophosphate in acetonitrile, in a Luggin capillary with a Vycor tip. For measurements in CH_2Cl_2, this Luggin capillary was inserted into a second Luggin capillary with Vycor tip filled with a 0.1 mol dm^{-3} [N(^{n}Bu)$_4$][B(C$_6$F$_5$)$_4$] solution in CH_3CN. For kinetic experiments, a glassy-carbon working electrode with surface area 3.1 mm^2 was also used. For the BAS C-27 instrument, data uncorrected for junction potentials were collected with an Adalab-PC and Adapt data acquisition kit (Interactive Microwave, Inc.) with locally developed software and analyzed with Hyperplot (JHM International, Inc.). For the BAS 100 instrument, data were collected with standard BAS 100 software. All measurements were conducted under a blanket of argon in a Faraday cage. Successive experiments under the same experimental conditions showed that all formal reduction and oxidation potentials were reproducible within 5 mV. All potentials in this study were experimentally referenced against the Ag/Ag$^+$ couple but were then manipulated on Excel to be referenced against Fc/Fc$^+$, as recommended by IUPAC.[38] Under our experimental conditions, the Fc/Fc$^+$ couple exhibited $E^{\circ\prime}$ = 0.087 V vs Ag/Ag$^+$, $i_{p,c}/i_{p,a}$ = 0.98, and ΔE_p = 74 mV in CH_3CN,and $E^{\circ\prime}$ = 0.263 V vs Ag/Ag$^+$, $i_{p,c}/i_{p,a}$ = 0.97, and ΔE_p = 81 mV in CH_2Cl_2.

Electrochemical Kinetics. Time-based CVs and OYSW voltammograms of 2.0 mmol dm^{-3} enol-enriched solutions of **4** in CH_3CN as well as in CH_2Cl_2 were recorded at a scan rate of 200 mV s^{-1} and frequency of 50 Hz. To overcome electrode fouling problems, manual adjustment of the amplitude of the internal standard, free ferrocene or the ferrocenyl wave of **4**, to identical peak current levels for each time-based run and conversion of the amended time-based peak currents to percent keto isomer allowed the collection of good interpretable kinetic data. CV decay currents in the free ferrocene internal marker and the ferrocenyl group peak number 1 of Figure 8 (and all other kinetic runs) were estimated by duplicating the decay current of the reduction half-wave of the ferrocene marker peak and overlapping it with the free ferrocenyl oxidation wave. Some broadening of the free ferrocenyl peak as well as amplitude manipulation was required for realistic overlaps and decay currents in the oxidation peaks. A realistic decay current was considered achieved once no obvious discontinuity was observable in each peak CV trace; i.e., no sharp corners or kinks are obvious when the decay current is superimposed on the CV trace. The decay current of peak 3, the enol ruthenocenyl half-wave, was estimated by duplicating and overlapping the ferrocenyl wavenumber 2 decay current with wave 3 (see Figure 8). The complete procedure for estimating decay currents is described in the Supporting Information using CH_3CN results as examples. For the Osteryoung square wave (OYSW) experiments, only peaks 1 and 2 were used to collect kinetic data, as demonstrated in Figure 8. Here, to measure peak currents, peak 1 from t = 126 s was copied and overlapped with all the other peak 1 and peak 2 peak positions at different times. Currents were then measured between peaks and neighboring peak profiles.

Acknowledgment. We acknowledge the NRF under Grant No. 2054243 and the UFS for financial support.

Supporting Information Available: Text and figures giving further explanations of electrochemisry experiments. This material is available free of charge via the Internet at http://pubs.acs.org.

OM700609Z

(34) *MINSQ, Non-Linear Parameter Estimation, V3.12*; MicroMath Scientific Software; Salt Lake City, UT, 1990.

(35) Jeffery, G. H.; Basset, J.; Mendham, J.; Denney, R. C. In *Vogel's Textbook of Quantitative Chemical Analysis*, 5th ed.; Longman Scientific and Technical: Essex, U.K., 1991; p 830.

(36) Martell, A. E. In *Stability Constants of Metal-Ion Complexes*, 3rd ed.; The Chemical Society: London, 1971; Special Publication No. 25, Part II, p 365.

(37) LeSuer, R. J.; Buttolph, C.; Geiger, W. E. *Anal. Chem.* **2004**, *76*, 6395.

(38) Gritzner, G.; Kuta, J. *Pure Appl. Chem.* **1984**, *56*, 461.